Journal of Environmental Management 193 (2017) 188–200

Contents lists available at ScienceDirect

Journal of Environmental Management

journal homepage: www.elsevier.com/locate/jenvman

Research article

A new hypervolume approach for assessing environmental risks

Denys Yemshanov [a, *], Frank H. Koch [b], Bo Lu [c], Ronald Fournier [c], Gericke Cook [d], Jean J. Turgeon [c]

[a] Natural Resources Canada, Canadian Forest Service, Great Lakes Forestry Centre, 1219 Queen Street East, Sault Ste. Marie, ON, P6A 2E5, Canada
[b] USDA Forest Service, Southern Research Station, Eastern Forest Environmental Threat Assessment Center, 3041 East Cornwallis Road, Research Triangle Park, NC, 27709, USA
[c] Natural Resources Canada, Canadian Forest Service, Great Lakes Forestry Centre, Sault Ste. Marie, ON, Canada
[d] USDA Animal and Plant Health Inspection Service, Centre for Plant Health Science and Technology, Plant Protection and Quarantine, Fort Collins, CO, USA

ARTICLE INFO

Article history:
Received 21 October 2016
Received in revised form
6 February 2017
Accepted 11 February 2017

Keywords:
Environmental risks
Non-dominant set
Hypervolume
Uncertainty
Asian longhorned beetle
Invasive species
Stochastic dominance

ABSTRACT

Assessing risks of uncertain but potentially damaging events, such as environmental disturbances, disease outbreaks and pest invasions, is a key analytical step that informs subsequent decisions about how to respond to these events. We present a continuous risk measure that can be used to assess and prioritize environmental risks from uncertain data in a geographical domain. The metric is influenced by both the expected magnitude of risk and its uncertainty. We demonstrate the approach by assessing risks of human-mediated spread of Asian longhorned beetle (ALB, *Anoplophora glabripennis*) in Greater Toronto (Ontario, Canada). Information about the human-mediated spread of ALB through this urban environment to individual geographical locations is uncertain, so each location was characterized by a set of probabilistic rates of spread, derived in this case using a network model. We represented the sets of spread rates for the locations by their cumulative distribution functions (CDFs) and then, using the first-order stochastic dominance rule, found ordered non-dominant subsets of these CDFs, which we then used to define different classes of risk across the geographical domain, from high to low. Because each non-dominant subset was estimated with respect to all elements of the distribution, the uncertainty in the underlying data was factored into the delineation of the risk classes; essentially, fewer non-dominant subsets can be defined in portions of the full set where information is sparse. We then depicted each non-dominant subset as a point cloud, where points represented the CDF values of each subset element at specific sampling intervals. For each subset, we then defined a hypervolume bounded by the outermost convex frontier of that point cloud. This resulted in a collection of hypervolumes for every non-dominant subset that together serve as a continuous measure of risk, which may be more practically useful than averaging metrics or ordinal rank measures.

Overall, the approach offers a rigorous depiction of risk in a geographical domain when the underlying estimates of risk for individual locations are represented by sets or distributions of uncertain estimates. Our hypervolume-based approach can be used to compare assessments made with different datasets and assumptions.

1. Introduction

Assessing risks of uncertain but potentially hazardous environmental events is a critical analytical step in deciding whether to monitor those events and, if necessary, develop appropriate mitigation strategies. Examples include introductions of unwanted insects and diseases (Aukema et al., 2011; Meyerson and Reaser, 2003), as well as negative ecological and economic impacts from fires, floods (Smith, 2013) and changing climate (Oppenheimer et al., 2014; Schneider et al., 2007). By nature, these events are uncertain and the sources of that uncertainty cannot be isolated sufficiently. In many cases, the uncertainty appears to be irreducible, such as the uncertainty associated with the spread of non-native harmful species (Melbourne and Hastings, 2009). Regardless, when predictive models (Carrasco et al., 2010; Hester et al., 2010; Koch et al., 2009; Yemshanov et al., 2009), including

* Corresponding author.
E-mail address: denys.yemshanov@canada.ca (D. Yemshanov).

http://dx.doi.org/10.1016/j.jenvman.2017.02.021
0301-4797/

ensemble analyses (Araújo and New, 2006; Cheung, 2001), are used to assess the potential impacts of such events, this uncertainty greatly curtails the decision support value of their results.

In general, the risk of an undesirable event can be represented by the probability of the event given a suite of conditions, along with some characterization of its consequences (Kaplan and Garrick, 1981). When knowledge about the event is poor, it may not be possible to depict the risk of the event with a single value. Instead, the risk can be depicted, at best, by a set (a distribution) of plausible values. For example, one way to estimate risks of invasion by an alien plant pest species in a spatial context is to simulate spatial stochastic scenarios of the invader's spread and calculate the probabilities of spread for each scenario, as well as the likelihoods under each scenario that populations of the pest will become established in newly-invaded locations. If the scenarios are assumed to have equal probability of occurrence, then this would essentially represent a distribution of likely outcomes with respect to the event of interest for a given site.

When multiple sites (or alternative events) must be compared, risk prioritization requires ordering the distributions of scenario-based risk estimates for each individual site (or event). In theory, if a distribution of plausible risk values can be approximated by a functional form (e.g., Gaussian), it is possible to describe that distribution by its first moments and depict these moments across the domain (e.g., as maps of mean risk values and their variance). This approach has been widely adopted in mean-variance investment analyses (Elton and Gruber, 1995; Keisler and Linkov, 2010; Linkov et al., 2006; Salo et al., 2011; Zhou et al., 2012). Indeed, these types of one- and two-dimensional estimates of risk are popular (see Sims and Finnof, 2013) because they make it possible to formulate and solve a decision-making problem with common optimization algorithms.

Unfortunately, the extent of knowledge about rare but potentially harmful events may be insufficient to properly determine the functional form of a distribution, and analysis may further be hindered by unknown limitations in the modeling technique or uncertainties in the data. Under such circumstances, comparisons of multiple observations in a geographical data set can only be done by considering the entire distribution (i.e., not just the first few moments) of estimated risk values for each of those observations. Ideally, this computationally complex task would be done using a metric that factors in the uncertainty of those multiple distributions, so that the final measure reflects the impact of both the expected magnitude of risk and its degree of variation.

In this paper, we propose a continuous metric that can be used to prioritize uncertain estimates of environmental risks that are depicted by plausible sets (distributions) of values that characterize the extent of impact or damage. Our metric is developed specifically for geographical assessments of environmental risks. It builds upon previous work (Yemshanov et al., 2012) in which we developed a risk metric utilizing the concept of stochastic dominance (SD). We first represent the sets of risk estimates for individual geographical locations in a data set (such as a collection of risk values for a given location generated under different modeling scenarios) by their cumulative distribution functions (CDF), so that every geographical location in the data set is characterized by its own CDF of risk estimates. We then find and rank distinct subsets of those spatial locations (i.e., of their CDFs) using the first-order stochastic dominance (FSD) rule. Ranking the subsets of spatial locations establishes their rank order along a gradient of risk. As described in Yemshanov et al. (2012), the subsets are termed “non-dominant” because each contains a group of CDFs that fail to dominate each other under the first-order stochastic dominance rule. These non-dominant subsets correspond to broad ordinal classes of risk that are ranked from high to low. Notably, for a rational decision-maker, a non-dominant subset would be perceived as a single risk class. This is because it is impossible to establish preference order relationships among the CDFs within a non-dominant subset (Levy, 1992; see more details in Section 2) due to uncertainty in the data, which makes the CDFs in the subset indistinguishable from each other in terms of FSD. This is why FSD is called a partial ordering approach: it facilitates ordering among, but not within, the subsets of a full set.

A relevant corollary is that when the data underlying a set of values, as represented by their CDFs, are highly uncertain, using FSD to compare all CDFs in that set will yield fewer and larger non-dominant subsets than if the underlying data were known more precisely. For decision makers, the ability to prioritize observations according to their risk will be constrained by the uncertainty in the underlying data. This restrictive behavior has important practical benefits: although FSD will yield imprecise and therefore coarse delineations of risk when applied to uncertain data, they are less likely to lead to erroneous decisions than estimates that fail to account for uncertainty and communicate false precision.

An acknowledged limitation of the SD approach is that it only provides an ordinal ranking of CDFs (and the corresponding risk gradations). As noted previously, non-dominant subsets are ordered from high to low risk under SD rules, but the actual difference in the levels of risk between any two subsets is unknown. For example, a geographical assessment of environmental risk (i.e., a risk map) developed using the SD approach would depict the risk levels of different geographic regions with ordinal ranks: 1st, 2nd, etc. Regions classified as 1st and 2nd rank might have very similar levels of risk, but in absolute terms, regions in the 2nd rank may actually be closer to regions in the 3rd rank, or even a much lower rank, than to regions in the 1st rank. Notably, an ordinal measure like SD offers only weak support for decisions where these kinds of fine-scale differences in risk may prove important, such as resource allocation to mitigate risk under tight budget constraints. A continuous measure, where the difference in the level of risk between the non-dominated subsets is quantified, would be far more suitable for such tasks.

Our objective is to describe a new approach, based on the concept of hypervolumes, which transforms the ordinal risk rank measure generated with the FSD rule into a continuous one. Briefly, we depict each non-dominant subset as a point cloud, where the points consist of the CDF values of each observation in the subset at defined sampling intervals. For each subset, we then define a hypervolume that is bounded by the outermost convex frontier of the point cloud and a chosen reference point. The result is a collection of nested hypervolumes, each of which quantifies volumetrically the region within the entire multi-dimensional risk space occupied by a non-dominant subset. Collectively, the calculated hypervolumes for these subsets act as a continuous measure of risk for the full set. As a continuous measure, it has another advantage over order-based risk metrics in that it can be used to prioritize and compare multiple assessments based on different datasets or risk assessment scenarios. We demonstrate the approach with a contemporary example: assessing the risk of human-assisted spread of the Asian longhorned beetle, an invasive forest pest (Haack et al., 2010; Nowak et al., 2001), in the Greater Toronto Area (Ontario, Canada).

2. Methodology

2.1. Assessing risks from scenario-based data

A set of uncertain risk estimates can be described by defining it as a stochastic variable, with a cumulative distribution function (CDF) of risk values x:

$$F(x) = P(X \leq x) \quad (1)$$

where CDF $F(x)$ returns the proportion of plausible estimates with the risk value less than x, which represents the probability of having a risk value less than or equal to x. If a risk estimate was certain (i.e., a single value x), its CDF would appear as a vertical line at x, such that CDF(x) returns a probability of 1 and any value other than x returns a probability of zero (Fig. 1a). Multiple certain estimates can be compared and ordered via equality/inequality operators. However, the CDF of an uncertain estimate is a monotonically increasing curve (Fig. 1b). Ordering of multiple uncertain estimates requires comparison of their CDFs.

One way to compare CDFs is by evaluating their pairwise dominance/non-dominance relationships (Levy, 1998) under the first-order stochastic dominance (FSD) rule. A CDF $F(x)$ dominates another CDF $G(x)$ by FSD if:

$$F(x) \leq G(x) \text{ for all } x \text{ and } F(x) < G(x) \text{ for one or more } x. \quad (2)$$

when $F(x)$ dominates $G(x)$, then $F(x)$ has a larger expected value, so $E(F(x)) > E(G(x))$. Notably, application of FSD also supposes that a rational decision-maker always prioritizes higher expected values than lower expected values (Levy, 1998) among all realizations of x. In our risk assessment case, this assumption generally holds because a decision-maker typically places greater priority on estimates of higher values (which denote greater risk of an undesirable event) than lower values. When dominance conditions for F and G (i.e., F over G or G over F) fail, it is impossible to establish a preference order relationship between F and G, and their CDFs become non-dominant to each other. Graphically, a non-dominance condition between F and G occurs when their CDFs cross each other at one or more points (Fig. 1b).

Dominance/non-dominance relationships among multiple observations (with uncertain estimates) in a set can be established via recursive pairwise comparisons of their CDFs. When the dominance condition fails between multiple pairs of CDFs, these CDFs form a non-dominant subset. For any non-dominant subset, there is always another CDF – or more commonly, another group of CDFs – that it dominates or by which it is dominated. This property has been used to establish rank order relationships between multiple CDFs (Yemshanov et al., 2012): a set of N CDFs can be ordered by finding distinct non-dominant subsets that delineate successively lower levels of risk (Goldberg, 1989). After the first non-dominant subset A_1 with the highest risk values is found in a full set N, it is assigned the highest ordinal risk rank of 1 and removed from the set temporarily. Then, the next non-dominant subset, A_2, is found from the remainder of the set, $N - A_1$, assigned a risk rank of 2, temporarily removed from set $N - A_1$, and so on. The procedure continues until all CDFs in set N are evaluated and assigned a corresponding rank.

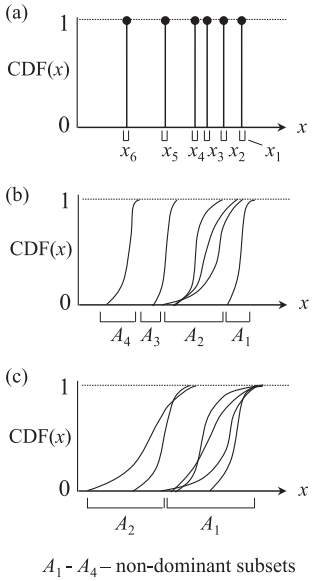

Fig. 1. Depicting certain and uncertain estimates of risk in CDF form: a) – certain estimates appear as vertical lines in CDF form and can be ordered using equality/inequality operators; b) ordering uncertain estimates requires comparison of their CDFs via dominance/non-dominance operators. Uncertainty in the underlying data, including in a portion of the data, causes the CDFs to cross each other and form non-dominant subsets, such as in A_2; c) more uncertainty provides more chances for CDFs to cross each other, yielding fewer, larger non-dominant subsets and further decreasing the number of distinct gradations of risk in the full set.

As mentioned earlier, an important property of the non-dominant subsets generated by this multiple comparison process is that their sizes (i.e., the number of CDFs each subset contains) are influenced by the amount of uncertainty in the underlying data. This is perhaps best demonstrated graphically. When the underlying data have little or no uncertainty, the slopes of the CDFs in the full set are steep (Fig. 1b), and dominance relationships may hold for CDFs with minute differences between their estimated values. Increasing the amount of variation in the data typically makes the CDFs shallower in slope and increases the chance that CDFs with similar estimated values will cross each other and subsequently form a non-dominant subset (Fig. 1b,c). As the size of the non-dominant subsets increases, there are fewer candidate subsets to which an observation can be assigned, so each subset typically contains more observations (i.e., more CDFs) than it would were the underlying data more certain. Furthermore, because no preference order relationships can be established within a non-dominant subset, all observations in each subset must be assigned the same risk rank value. In short, using less precise data leads to fewer and larger non-dominant subsets, which subsequently provide coarser risk gradations and fewer distinct risk classes (Fig. 1). These coarser gradations have important implications for decision-making because they make it difficult to distinguish just a small (i.e., restricted) number of observations with the highest (or lowest) risk. Consequently, when determining their management priorities based on the risk, decision-makers must devote enough resources to address all of the comparatively larger groups of observations ranked as high risk under the FSD rule.

2.2. Ordering the non-dominant subsets with a hypervolume metric

Stochastic dominance relationships can only provide a partial rank ordering of the non-dominant subsets in a full set. Ideally, each subset would be characterized with a continuous measure that defines its absolute position in the same dimension space. Such a continuous metric would enable comparison of different risk rankings within the same frame of reference.

One approach to comparing non-dominant subsets is to use performance indicators (Knowles and Corne, 2002). Essentially, this means comparing any two non-dominant subsets in terms of their indicator values. The indicator must be able to show quantitative differences between the subsets and also accommodate a diversity of subset configurations. We propose using a hypervolume indicator (HV), also called the S-metric (Fleischer, 2003) or Lebesgue measure (Laumanns et al., 2000). The hypervolume metric has seen increasing use in multi-objective optimization to assess the positions of convex Pareto-optimal sets (Brockhoff et al., 2008; Fonseca et al., 2006) (Fig. 2). Formally, the hypervolume of a non-dominant subset A, $A \subseteq N$, is defined as the hypervolume of the k-dimensional space that is dominated by subset A and is bounded by a reference

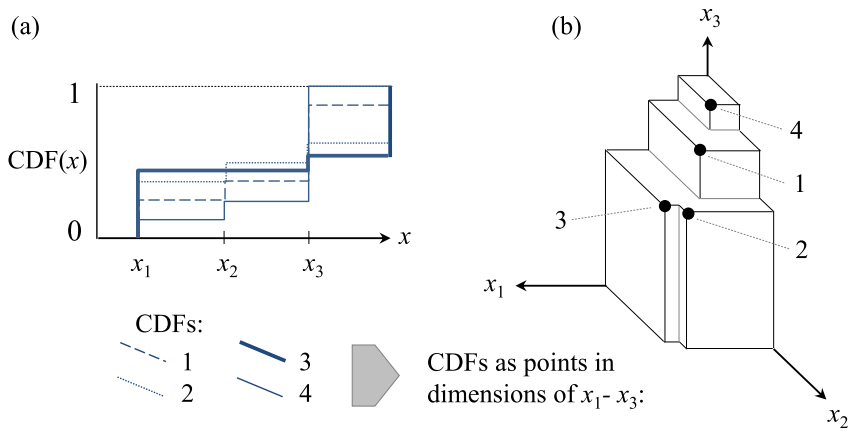

Fig. 2. Geometric illustration of the hypervolume concept: a) an example non-dominant subset of four cumulative distribution functions (CDFs) sampled at three discrete intervals, x_1, x_2 and x_3: CDF1 (0.25, 0.375, 0.875), CDF2 (0.375, 0.5, 0.625), CDF3 (0.45, 0.45, 0.55) and CDF4 (0.125, 0.25, 1); b) depicting the set of CDFs 1–4 as a point cloud in dimensions of CDF sampling intervals x_1 - x_3. The hypervolume of the set (i.e., subset) of CDFs 1–4 is a volume under the convex frontier of points 1–4 and a chosen reference point (0,0,0).

point $r = (r_1, \ldots, r_k)$:

$$\mathrm{HV}(A) = \lambda\left(\bigcup_{a \in A} [f_1(a), r_1] \times [f_2(a), r_2] \times \ldots \times [f_k(a), r_k]\right) \quad (3)$$

where $\lambda(S)$ is the Lebesgue measure of a subset A and $[f_1(a), r_1] \times [f_2(a), r_2] \times \cdots \times [f_k(a), r_k]$ is the k-dimensional hypercuboid consisting of all points that are dominated by any point a in subset A but not dominated by the reference point r (Brockhoff et al., 2008). Due to its unique properties (Zitzler et al., 2003), a subset with a larger hypervolume presents a better trade-off between the dimensions in which the hypervolume was measured than subsets with smaller hypervolumes.

The HV indicator has several favorable mathematical properties, including that it complies with Pareto optimality (Back et al., 1997; Beume et al., 2007; Zitzler et al., 2003; Zitzler and Thiele, 1998). The Pareto optimality concept describes a vector of multiple criteria for which performance with respect to one risk criterion cannot be improved without sacrificing performance with respect to at least one other criterion (Pareto, 1971). The Pareto-optimal set represents the trade-off between the criteria and is defined with respect to the concept of non-dominance between points in criteria space (Back et al., 1997; Zitzler et al., 2003). HV is also known to be monotonic with respect to Pareto dominance, thereby guaranteeing that the Pareto-optimal set achieves the maximum hypervolume possible (Zitzler et al., 2003). This property is beneficial in our case, where a decision-maker needs to compare multiple non-dominant subsets. The hypervolume also tends to prioritize convex sets (Zitzler and Thiele, 1999) and is maximized when the set contains all Pareto-optimal points (Fleischer, 2003) (Fig. 3a). Among different non-dominant subsets, HV tends to better represent boundary conditions in the Pareto-optimal set (Deb et al., 2005). A single-point set with the hypervolume equal to a Pareto-optimal set would have higher linear measurements in the dimensions 1, 2, …, k than the points in a Pareto set (Fig. 3b).

To implement the HV indicator, we characterize each non-dominant subset that has been delineated with the FSD rule by sampling the CDFs it contains at k discrete intervals. Thus, we represent each CDF, a member of a non-dominant subset, as a point in a k-dimensional space, where each dimension represents the kth sampling interval of the CDFs and the point's coordinate in the kth dimension is the CDF value at kth sampling interval (Fig. 2). Geometrically, a non-dominant subset of CDFs forms a k-dimensional point cloud in the dimensions of these sampling intervals.

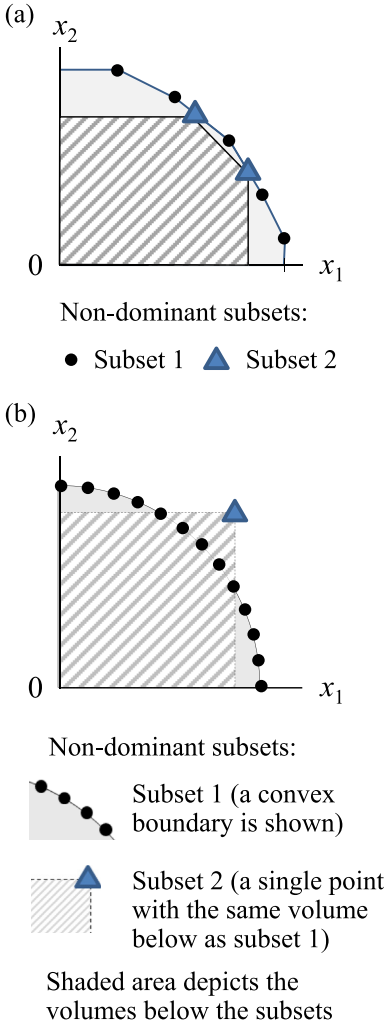

Fig. 3. Geometric two-dimensional illustration of basic hypervolume properties: a) a non-dominant subset with more Pareto-optimal points has larger hypervolume than a subset with fewer Pareto optimal points; b) A single-point subset with a hypervolume equal to a Pareto-optimal subset has higher linear measurements in the hypervolume dimensions than any point in the Pareto-optimal subset.

For each subset, we define a hypervolume that is bounded by the outermost convex frontier of that point cloud (Fig. 2b). For multiple non-dominant subsets, this results in a collection of hypervolumes that define and quantify the regions occupied by the non-dominant subsets in a continuous space.

When CDFs are sampled at a large number of discrete intervals, the hypervolume must be calculated for a high-dimensional case. This task is computationally demanding, which is one of the main reasons HV has seen limited application before now (Emmerich et al., 2005; Huband et al., 2003; Knowles et al., 2006). Recently, several fast HV algorithms have been proposed (Bradstreet et al., 2008, 2010; Bringmann and Friedrich, 2010; Fonseca et al., 2006; While et al., 2006; Zitzler, 2001). For this study, we used the exact HV algorithm from While et al., (2005).

2.3. Case study: assessing risks of human-mediated invasion of Asian longhorned beetle, a high-threat alien pest in Greater Toronto, Canada

We illustrate the hypervolume approach with a case study that assesses risk of potential invasion of Asian longhorned beetle (ALB, *Anoplophora glabripennis* (Motschulsky) (Coleoptera: Cerambycidae)) beyond the boundaries of a quarantined area. ALB has been introduced to the eastern U.S. and Canada and could potentially have a catastrophic impact on several genera of hardwood trees across North America, particularly in urban forest environments (Nowak et al., 2001). It was initially discovered in 1996 in New York (NY) (Haack et al., 1996, 1997), and subsequently has been found in Chicago (IL), Clermont County (OH), Jersey City (NJ), Carteret (NJ), and Worcester (MA) (APHIS, 2013; Haack et al., 2010; Meng et al., 2015; Poland et al., 1998; Shatz et al., 2013; Trotter and Hull-Sanders, 2015). In Canada, the first infestation was discovered in 2003 in the Greater Toronto Area (GTA, ON) (Hopkin et al., 2004; Turgeon et al., 2010). All of these introductions involved specimens that had originated in China (APHIS, 2005; Carter et al., 2009). Since 2001, the species has also been found in Europe (EPPO, 2008; Maspero et al., 2007; Straw et al., 2015; van der Gaag and Loomans, 2014). In invaded landscapes, maple (*Acer* spp.) is the preferred host of ALB, but the beetle also attacks and completes its development in birch (*Betula* spp.), poplar (*Populus* spp.), elm (*Ulmus* spp.), willow (*Salix* spp.) and another half dozen tree genera (CFIA, 2014; Faccoli and Favaro, 2016; Haack et al., 2010; Hu et al., 2009; Lingafelter and Hoebeke, 2002; Meng et al., 2015; van der Gaag and Loomans, 2014; Wang et al., 2005; Williams et al., 2004), making it one of the world's most threatening and undesirable invasive forest pests (Haack et al., 2010; Nowak et al., 2001). Eastern North America seems to be particularly vulnerable because of the ubiquity of maple and suitable climatic conditions (Peterson and Scachetti-Pereira, 2004). If the further spread of ALB in North America is not contained, its impact could extend to many commercial sectors that use the aforementioned tree genera (Haack et al., 2010; Hu et al., 2009).

Some early detection techniques have been developed for ALB (Nehme et al., 2014; Smith and Wu, 2008), but visual inspection of trees for signs of attack remains the only practical method (Turgeon et al., 2007, 2010). An initial 152 km^2 regulated area in the GTA was declared free of *A. glabripennis* in April 2013 by the Canadian Food Inspection Agency (the agency in charge of the eradication program) after five years of negative survey results (CFIA, 2013). A few months later, another breeding population, suspected of being a satellite infestation of the population discovered in 2003, was discovered outside that regulated area (Turgeon et al., 2015). The regulated quarantine area of this residual infestation is approximately 46 km^2 (Fig. 4). Treatment of this infestation consisted of removing all high-risk suitable host trees (infested or not) within

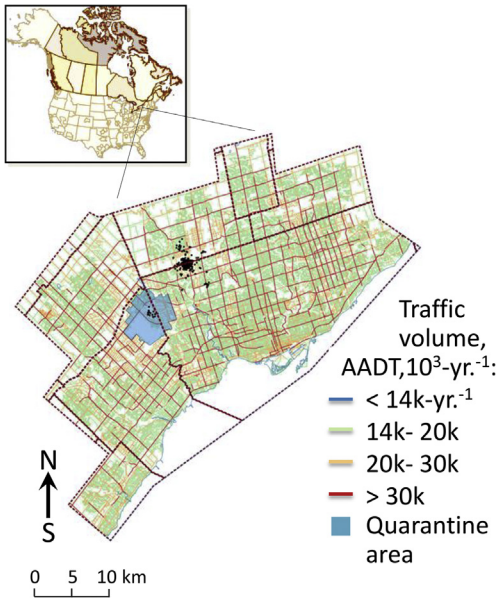

Fig. 4. Case study area (Greater Toronto, ON, Canada): local street traffic (a proxy of human-mediated spread of invasive species), average adjusted daily traffic counts (AADT, 10^3 yr.$^{-1}$).

800 m of any tree found to be infested. The potential for extensive further damage, high eradication costs and the need to maintain market access, necessitate the assessment of the risk that ALB might have spread beyond this quarantine area.

ALB is known to have slow natural spread rates (Smith et al., 2001, 2004): 80% of a population is expected to spread 300 m or less by its own biological means (Favaro et al., 2015; Straw et al., 2016). However, most recent ALB introductions have been caused by humans (Carter et al., 2009). Growing anecdotal evidence suggests that the pest may hitchhike on slow-moving vehicles (Trotter and Hull-Sanders, 2015; Turgeon, pers. obs.), similar to the documented spread of another invasive forest insect, the emerald ash borer (*Agrilus planipennis* Fairmaire; Coleoptera: Buprestidae), in urban settings (Buck and Marshall, 2008). In most cities and towns, including the GTA, local road traffic (involving both passenger and commercial vehicles) accounts for a large portion of the area-wide movement of people and goods. Consequently, road traffic has been recognized as a reasonable proxy for a variety of local economic activities (SACTRA, 1999). This suggests that local vehicle traffic could be a potential vector for ALB spread via an urban street network. To assess risk of ALB spread in the GTA, we used local road traffic data from the TrafficMetrix dataset, which describes traffic flow patterns in Canada and the U.S. (Tetrad Inc, 2014). We interpolated these volumes to the networks' linear street segments such that each individual segment was assigned a traffic volume based on nearby points in the dataset (see Cook and Downing, 2013). The ESRI StreetMap dataset (ESRI, 2014) served as the geospatial foundation for the linear features comprising the Canadian and U.S. networks (Cook and Downing, 2013), which we combined into a single network.

We used volumes of local road traffic as a measure of activities that could cause human-mediated ALB spread (see description in Appendix S1). The GTA street network was divided into 400 × 400-m blocks, each representing a potential survey site, and then we used the local traffic volume data to estimate a matrix of probabilities of ALB spread from block to block via the network. Our choice of spatial resolution was dictated by the current ALB response protocol in the GTA, which mandates immediate

eradication and host tree removal within at least a 400-m distance of any infested location, depending on the number of infested trees (B. Gasman, CFIA, pers. comm.). An ALB population can survive on a few host trees (Turgeon et al., 2015), so the local host density was not used to adjust the establishment rate value (Appendix S1).

2.4. Model calibration and sensitivity analysis

The model of ALB invasion was used to calculate $p_{j\ est}$, the likelihood that ALB will spread to and become established in a destination location j, with subsequent impact on the host trees present in j. Importantly, the arrival rates (i.e., the φ_j values) generated by the model (see Eqs. S1-S3 in Appendix S1) were relative values that required calibration. We calibrated the model so that it generated successful infestations at a rate that agreed with historical rates of ALB infestation in the GTA. Historically, ALB has established an average of 12 new satellite infestations over the survey period (Turgeon, unpubl. data). For the calibration, we first simulated the likelihoods of ALB spread and subsequent establishment, $p_{j\ est}$. Next, we created new infestations via uniform random draws against the $p_{j\ est}$ values. We then compared the number of created infestations to the historical rate and calibrated the λ value in Eq. S(1) (Appendix S1) to match the model-based rate of roughly 12 new infestations per year throughout the GTA.

To characterize the uncertainty of ALB spread and establishment, we estimated spatial patterns of $p_{j\ est}$ values for 5000 stochastic scenarios. Thus, each 400 × 400-m block j was characterized by a distribution of 5000 plausible $p_{j\ est}$ values, which served as our basis for illustrating the hypervolume approach.

Spatial assessments of risk often rely on interpolated data, so interpolation represents another potential source of uncertainty. We explored the response of the HV metric to errors introduced by interpolation. For each of 5000 realizations of ALB spread and establishment, we modified the $p_{j\ \mathrm{est}}$ values at individual spatial locations by adding symmetric uniform random variation within a fixed proportion of the actual p_j value, i.e.:

$$p_{j\ \mathrm{int}} = p_{j\ \mathrm{est}}(1 \pm \mathrm{uniform}[0;1]^{*}\alpha) \quad (4)$$

where α is a scaling coefficient that denotes this proportion. Essentially, the transformation in Eq. (4) preserves the mean p_j values and does not change the relative positions of the CDFs, but smooths local imperfections in the CDF shapes.

We also evaluated the response of the HV values when adding uncorrelated uniform random noise to the data. We altered the p_j values in each of model realizations by adding symmetric uniform random deviation error, i.e.:

$$p_{j\ \mathrm{alt}} = p_{j\ \mathrm{est}} + \mathrm{uniform}[0;1]^{*}\beta \quad (5)$$

where β is a scaling coefficient. We then compared the HV values of the altered scenarios with the estimates calculated with the non-altered p_j values.

3. Results

We first depict the geographical patterns of spread and the HV (i.e., continuous) and ranked (i.e., ordinal) risk measures based on delineation of non-dominant subsets. To make the two measures comparable, we rescaled the ranked risk values as $1 - rank/\max[rank]$, so that the ranks denoting the highest risk of ALB spread and establishment are 1 and the lowest-risk rank values are 0. We also calculated the kth root of the HV measure, $HV^{1/k}$, which similarly varies within a 0–1 range and is therefore more compatible with the rescaled rank values than the original HV measure. The map of mean $p_{j\ \mathrm{est}}$ values, which can be interpreted as a basic risk map, depicts semi-concentric patterns of spread probabilities that decline with distance from the quarantine zone (Fig. 5a). The map suggests that risk of infestation is high ($p_{j\ \mathrm{est}} > 0.005$) only at sites proximal to the quarantine zone. As expected, the $p_{j\ \mathrm{est}}$ values appeared to be uncertain over the 5000 scenarios (Fig. 5b). The map of the standard deviations follows the same general pattern as the mean $p_{j\ \mathrm{est}}$ map, however many sites adjacent to the quarantine zone exhibit comparable variation in the $p_{j\ \mathrm{est}}$ values to sites further away from the zone (Fig. 5b). This occurs because arrivals of ALB at sites adjacent to the quarantine zone are more certain than arrivals at more remote sites, which decreases their standard deviation estimates.

The map of HV values (Fig. 6a) shows considerably more area under high and medium risk than the map of mean $p_{j\ \mathrm{est}}$ values. In fact, regions of medium risk with HV values between 0.6 and 0.8 occupy roughly the same area as occupied by low-risk regions ($0.0001 < p_{j\ \mathrm{est}} < 0.001$) in the map of $p_{j\ \mathrm{est}}$ values. The HV method tends to assign higher risk to sites with more uncertain estimates.

The rescaled rank and HV measures show similar geographical patterns of risk, although the $HV^{1/k}$ map shows fewer high-risk locations (Fig. 6a,b). The similarities in the rescaled rank values and $HV^{1/k}$ values indicate that these metrics are correlated (see Fig. 7a). We likewise found a consistent relationship between the

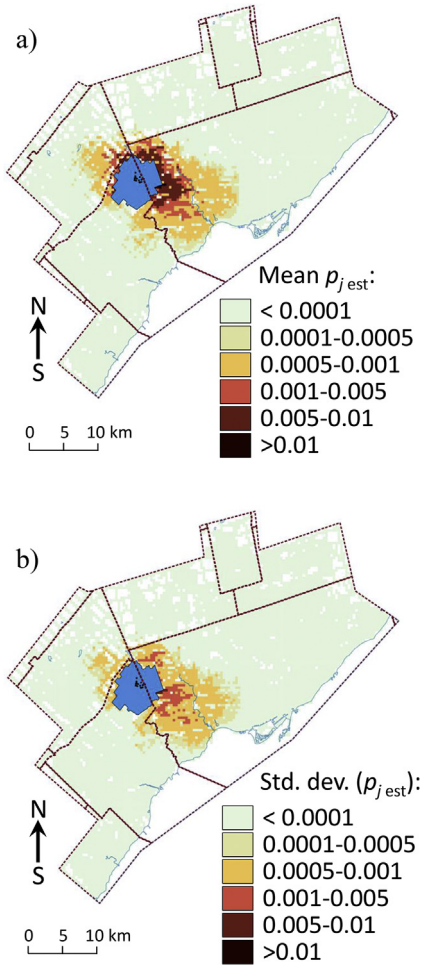

Fig. 5. Geographical pattern of the likelihood of ALB spread and establishment in the study area: a) map of the mean likelihood of spread and establishment, $p_{j\ \mathrm{est}}$ (an average of 5000 model realizations); b) map of the standard deviation of the $p_{j\ \mathrm{est}}$ values.

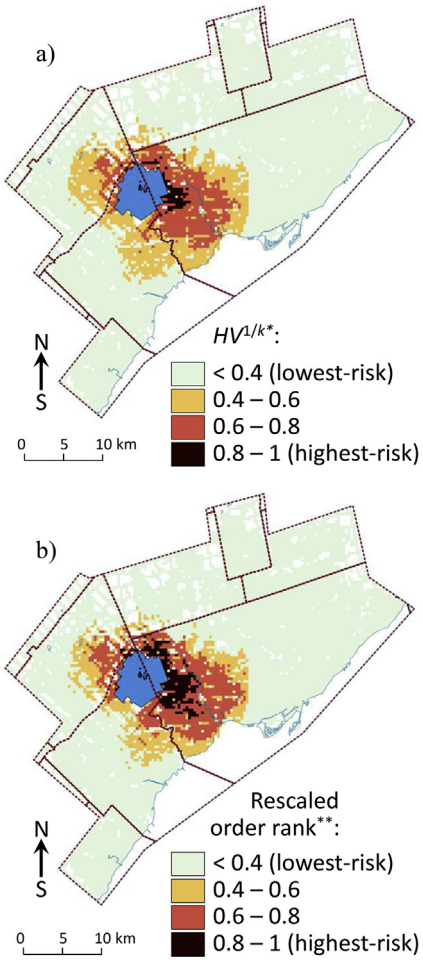

Fig. 6. Geographical patterns of the hypervolume metric and the rescaled risk ranks: a) $HV^{1/k}$ values; b) rescaled risk ranks. In both cases, values close to 1 denote locations with the highest risk of ALB spread and subsequent establishment.

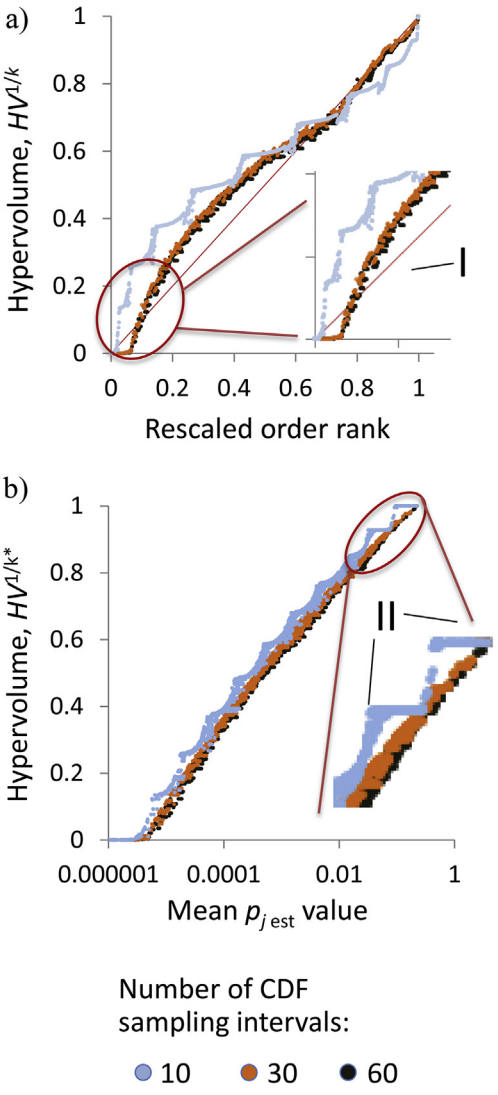

Fig. 7. Relationships between the hypervolume metric, rescaled risk rank and mean $p_{j\ est}$ values: a) hypervolume versus risk rank. A 45-degree line denotes the equivalence between the rescaled rank and the HV measures. Callout I shows a close-up of the lowest-risk estimates with near-zero probabilities of spread; b) hypervolume as a function of the mean $p_{j\ est}$ values. Points represent distinct geographical locations. Callout II shows a close-up of the highest-risk locations. The conditions when many distinct p_j values have fewer distinct HV gradations appear as steps in the graph.

HV and $p_{j\ est}$ values (Fig. 7b). Although the rescaled ranks and $HV^{1/k}$ values are positively correlated (Fig. 7a), high-risk ranks appear to have comparatively lower $HV^{1/k}$ estimates, and this trend reverses with low-risk ranks (except in the case of very low values, as noted below). This is expected: In the rank order set, subsequent rank values denote nested non-dominant subsets, but the increment between adjacent subsets is always the same. Alternatively, the HV measure quantifies the region occupied by each subset in dimensions of the CDF sampling intervals, and thus takes into consideration the magnitude of differences between the non-dominant subsets. For example, many locations with very low risk values, $p_j < 0.0001$, were identified as distinct ordinal ranks, however when differences between the CDFs were taken into account they were assigned near-zero HV values (Fig. 7a, callout I).

We also explored the sensitivity of the hypervolume measure to the number of CDF sampling intervals and compared the $HV^{1/k}$ estimates for the non-dominant subsets of CDFs sampled at 10, 30 and 60 intervals (Fig. 7). When the number of CDF sampling intervals is small, the differences between the HV and rank values increase rapidly (Fig. 7a). In the case of a scenario with few CDF sampling intervals (e.g., $k = 10$), the resolution of the underlying data is coarse, so the shapes of the CDFs are also coarse, thereby limiting the number of distinct HV values and corresponding risk gradations. This aspect was evident in our scenario with ten CDF intervals, which identified fewer distinct HV values for high-risk locations than the scenarios with 30 and 60 intervals (Fig. 7b, callout II). Coarser HV gradations appear as steps in Fig. 7b: Many elements have different mean $p_{j\ est}$ values but the same HV values. This indicates that ten CDF sampling intervals do not provide enough information to establish preference order relationships between elements with only small differences in their $p_{j\ est}$ values.

In general, errors (i.e., uncertainty) associated with interpolated data appear to have a relatively modest impact on HV values. Table 1 shows the number of non-dominant subsets that were delineated when we simulated spatial errors that are typical of interpolated data (see Eq. (4)). Higher levels of added symmetric noise in the data provided more chances for the CDFs to cross each other, which led to the delineation of fewer non-dominant subsets than with unaltered $p_{j\ est}$ values (Table 1a,b). Nevertheless, while the number of non-dominant subsets changed, this particular transformation did not change the relative positions of CDFs along the gradient of high-to-low risk. Rather, the HV estimates based on

Table 1
Impact of the CDF sampling rate, interpolation and uniform random noise on the number of delineated non-dominant subsets in the data.

Scenario	Number of CDF sampling intervals[a]		
	10	30	60
a) Unaltered $p_{j\ est}$ values			
	1577	382	319
b) Interpolated data			
α[b] = 0.1	1516	361	288
$\alpha = 0.5$	746	304	245
c) Data with added uniform random noise			
β[c] = 0.01	1291	313	234
$\beta = 0.05$	903	253	184

[a] Sampling from a distribution of 5000 $p_{j\ est}$ values at intervals roughly corresponding to 10, 30 or 60 percentile points.
[b] See Eq. (4) for data transformation description.
[c] See Eq. (5) for data transformation description.

the interpolated data ($\alpha = 0.1$, $\alpha = 0.5$) were very close to the HV values in the unaltered scenario (Fig. 8a). This behavior was anticipated because the uniform variation added to the p_j values was symmetric and linearly proportional to the original p_j values.

The HV estimates reacted differently to the addition of non-correlated uniform random noise to the data (Fig. 8b). In this case, the symmetric uniform variation that was added to the p_j values did not depend on the p_j value, and as expected, the most noticeable impact was associated with $p_{j\ est}$ values below the maximum noise level (β). While rank order relationships could still be established among the altered values, $p_{j\ alt}$ that fell below this noise level, information about the lowest risk values was masked by the noise. This was demonstrated by the HV metric (Fig. 8b), which leveled off in the altered scenarios ($\beta = 0.01$, $\beta = 0.05$) at some positive value corresponding to the average amount of added uniform noise in the data. By comparison, when the $p_{j\ est}$ values were unaltered, the lowest-risk HV values were close to zero. Because the amounts of added random variation were very small, the HV values for high-risk sites were unaffected. However, in both altered scenarios the added uniform variation reduced the number of non-dominant subsets that could be delineated from the data (Table 1).

4. Discussion

Many risk analysts consider the use of probabilities in risk assessments to be an appropriate way to quantify uncertainties

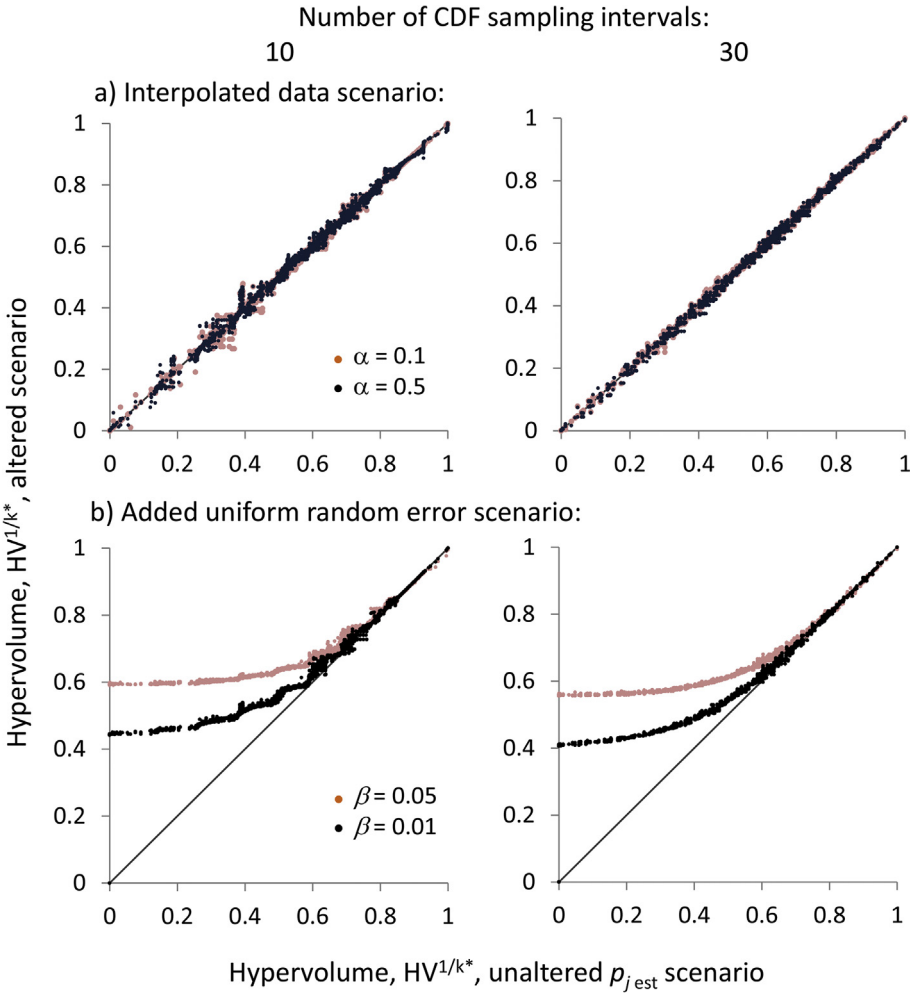

Fig. 8. Impact of data transformations on the hypervolume measures: a) impact of data interpolation. The x-axis shows the HV values in the unaltered scenario and the y-axis shows the HV values in the scenarios ($\alpha = 0.1$, $\alpha = 0.5$) based on interpolated data; see Eq. (4) for data transformation algorithm; b) Impact of added uniform random error. The x-axis shows the HV values in the unaltered scenario and the y-axis shows the HV values in the scenarios ($\beta = 0.01$, $\beta = 0.05$) with added random noise; see Eq. (5) for data transformation algorithm.

about unknown undesirable events (Aven, 2010). However, probabilities – in the objective, frequentist sense – do not provide an adequate characterization of epistemic uncertainties (i.e., uncertainties that arise from a lack of knowledge about the phenomena of interest, rather than intrinsic variability), for which it is impossible to determine an underlying probability distribution (Paté-Cornell, 1996). It is thus no surprise that risk assessments based on incomplete or ambiguous information (i.e., that have high levels of epistemic uncertainty) are often viewed skeptically by decision-makers tasked with using these assessments to implement risk mitigation measures (Brugnach et al., 2007; Walker et al., 2003; White et al., 2015). It should also be no surprise that the results of quantitative risk assessments are seldom accepted as the sole basis for making risk mitigation decisions (Apostolakis, 2004; Aven and Zio, 2014; Goerlandt et al., 2015). Aven (2010) argued that epistemic uncertainties can be communicated effectively to decision-makers using subjective probabilities, which provide expert-qualified judgments about unknown quantities (e.g., what is your degree of belief that a model parameter exceeds value x?). Regardless, if the uncertainties are characterized separately from the primary measure of risk, there is some danger that they will not be incorporated into the decision-making process, which could lead to erroneous choices (Yemshanov et al., 2015). The ability to incorporate uncertainties, including epistemic uncertainties, directly into output risk values is one of the primary advantages of an SD approach (Canessa et al., 2016; Yemshanov et al., 2012). Indeed, the SD concept originally came to prominence in economics and finance as a robust way to order risky investment choices that, despite being uncertain for some value of interest (e.g., the expected return on investment), could still be compared in terms of their ranges of *possible* values (Levy, 1992, 1998). In particular, the FSD metric is consistent with distortion risk measures used in financial management, such as the Value-at-Risk (Jorion, 1997), which considers the CDF of returns on an investment portfolio (De Giorgi, 2002).

A consideration of the entire distribution is also beneficial when all sources of uncertainty in the underlying data (such as Type I/II errors) cannot be identified. While various other statistical tests, such as Kolmogorov-Smirnov's (Peacock, 1983; Smirnov, 1948), Kuiper's (Kuiper, 1962) or earth mover's distance (Cohen and Guibas, 1997; Rubner et al., 2000), can be used for pairwise comparisons of CDFs, they do not always preserve the preference order relationships among distributions. By contrast, the FSD condition of $F(x)$ over $G(x)$ ensures that any realization of x in F would be preferred to G, i.e., if F dominates G by FSD, any rational decision-maker would prefer F to G.

Other common risk measures that factor in uncertainty are based on distribution moments, such as the certainty equivalent (Gerber and Pafumi, 1998), which is a weighted average of mean and variance, or more simply, depicting risk in dimensions of the mean and its variance (Markowitz, 1952). However, both approaches require the distribution to conform to a known functional type. Because the non-dominance conditions in our HV approach (and the underlying FSD approach) are estimated with respect to all variation in the distribution (i.e., the entire CDF), they do not depend on the distribution's functional type (Fishburn and Vickson, 1978) and do not rely on the distribution moments, so the methods can be used with poor data. This has another interesting practical benefit over measures based on distribution moments: the delineations of risk become coarser when the underlying information is poor. Poor data quality limits the ability to differentiate CDFs and lead to coarse delineation of risk priorities. Coarser gradations of risk provide decision-makers with fewer prioritization choices. This creates a feedback between the quality of the data and a decision-maker's ability to differentiate fine gradations of risk. When the number of estimated risk levels is too few to make sensible allocation of resources, indicating an inability to distinguish between these elements sufficiently, this may suggest deferring a decision action until a more confident assessment of risk is possible.

In spite of their advantages, a key limitation of SD approaches is that they can only generate ordinal risk ranks (Yemshanov et al., 2012). Ordinal measures of risk offer limited decision-making utility because they can only prioritize a *sequence* of decision-making actions but do not indicate how much riskier one action may be than another. Our hypervolume measure helps address this issue by establishing quantitative gradations of risk. By giving decision-makers more descriptive (i.e., quantitative rather than ordinal) information on risk – even if the net result is a smaller set of prioritization choices – our HV approach lends more rigour to assessments of risk in time-critical situations than estimates based on ordered ranks.

The hypervolume approach can be adapted to a broad range of environmental applications; for instance, it could be used to assess and map risks of pest and disease outbreaks, fires, floods, pollution scenarios and other hazardous events. The HV metric can be used in monitoring routines where a decision-maker needs to prioritize uncertain estimates based on sampled uncertain data. Consider a collection of monitoring plots where each plot is sampled at a number of measurement points. Each plot is essentially represented by a distribution of imprecise measurements, with the error structure of the sampling effort unknown. These distributions can be ordered with the HV method.

The HV measure can also be applied as a priority measure to guide invasive species control and eradication efforts in the same manner as other common risk measures, such as probabilities of species spread. For instance, risk priority measures are sometimes used as input parameters for optimization-based models that allocate resources for detection and management (see Sims and Finnof, 2013). Our HV measure can serve as an input parameter for optimization, and since it is based on FSD comparisons, has the added advantage of preserving preference order relationships between levels of risk (i.e., between non-dominant subsets of the full set of risk values) (Levy, 1998). Notably, measures based on averaging do not always preserve these preference order relationships, and may not guarantee that a rational decision-maker will, as expected, prioritize a subset with a higher mean risk value over one with a lower mean risk value. In some cases, a risk-averse decision maker may opt for an alternative characterization of risk that does not involve ordering subsets by non-dominance, but instead uses the worst-case combination of risks in a subset. It is possible to calculate the hypervolume measure for a worst-case scenario. In this case, one would need to construct a CDF that delineates an upper bound of a non-dominant subset, which represents the worst combination of risks for all elements of the subset (Fig. 9a). In turn, hypervolume measures can be calculated for this and all of the other upper bound CDFs. The hypervolume of an upper bound CDF is expected to be higher than the hypervolume of an entire non-dominant subset, however the difference may depend on the structure of the subset and the number of elements in the subset. For example, in our case study, differences between the upper bound and entire-subset-based HV estimates appear to be relatively minor (Fig. 9b) because the number of elements in the non-dominant subsets typically was small. For other data types, the upper bound HV values may show more distinct patterns. These estimates can provide practical insights when a decision-maker is risk-averse and therefore perceives risk as a worst-case scenario.

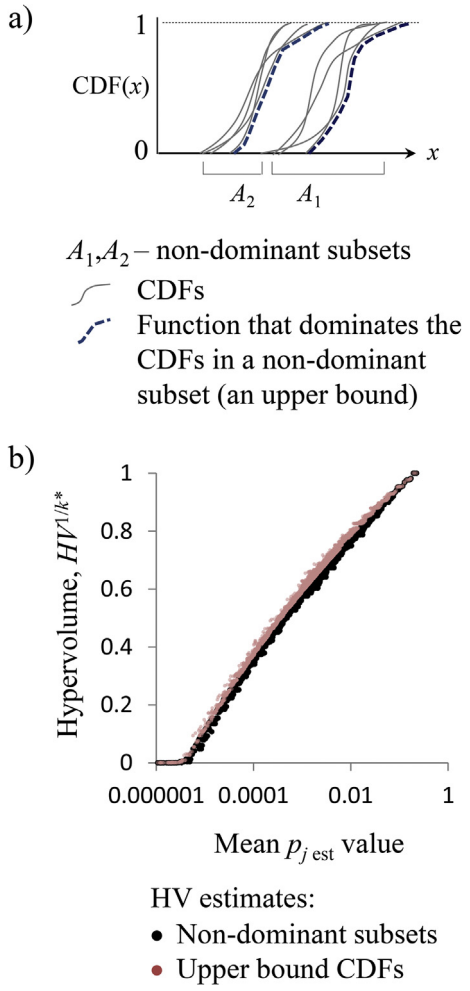

Fig. 9. Characterization of a non-dominant subset with the CDF that delineates an upper bound of a subset (i.e., the worst-case combination of the CDFs in the non-dominant subset): a) An upper bound concept; b) A comparison of the HV values estimated for non-dominant subsets with the hypervolumes of their upper bound CDFs. X -axis denotes mean $p_{j\ est}$ values and Y-axis shows the hypervolume estimates.

4.1. Practical use of the hypervolume metric to prioritize environmental risks

Previous use of the HV metric has been mostly confined to work in the area of multi-objective optimization for computation and engineering design (Wu and Azarm, 2001; Zitzler et al., 2003), and is relatively new in ecological and environmental risk assessment. The HV metric is built upon previous stochastic ordering techniques, but also improves upon them as a continuous measure estimated in the dimensions of the CDF sampling intervals. Significantly, the HV metric can be used in conjunction with not only SD, but any risk ordering technique that estimates multi-criteria frontiers or Pareto-optimal subsets (Yemshanov et al., 2013).

In practical terms, uncertainty in the underlying data influences the associated HV metric in two distinct ways. As described earlier, coarser information (regarding model formulation, parameters, etc.) leads to delineation of fewer non-dominant subsets and coarser gradations of risk. Secondly, larger non-dominant subsets with more elements typically have larger hypervolumes than smaller subsets or single elements with the same expected values. This is a result of a unique property of the HV metric: the hypervolume of a convex non-dominant subset is always bigger than the volume of any single element in the subset (Fig. 3a). Hypervolumes can be calculated for subsets with any number of elements, which enables comparison of different risk assessment scenarios (as long as the same CDF sampling intervals are used).

The method has simple data requirements: a vector of S scenarios, where each scenario is represented by N uncertain risk estimates. For FSD and HV calculations, the number of sampling points N should be sufficient to represent the shape of CDFs. The maximum data size is limited by the computational complexity of the pairwise CDF comparisons and HV calculations. Current capacity on the order of N~10^5-10^6 is sufficient for many environmental applications but could be increased further by parallelizing the pairwise FSD calculations.

Sometimes, the lack of data in risk assessment models is compensated by interpolation techniques. Interpolation smooths the data but may distort the shape of the CDFs and influence the delineation of the non-dominant subsets. Ideally, the HV calculations should use the data in their real shape without interpolation.

The choice of the underlying risk metric is highly important because it may change the interpretation of the uncertainty and subsequently the delineations made with the HV metric. Moreover, if the risk metric takes into account costs or is represented in a monetary equivalent, then the HV metric could be used effectively to prioritize cost-effective management actions in geographical environments. The method is also sensitive to the number and spacing of the CDF sampling intervals. A larger number of CDF sampling intervals could provide more opportunities for CDFs to cross each other, creating fewer non-dominant subsets. For example, the CDF estimates based on 10 sampling intervals in our study had 4.9 times more non-dominant subsets than the estimates based on 60 sampling intervals (Table 1a). Using percentile points to sample CDFs is a good general strategy, but other factors, such as which percentile points are most important for decision-making, should be considered.

The dominance conditions can also be affected by sampling errors in the left tail of distributions. The importance of proper sampling of the left tail of distributions was illustrated in the sensitivity scenario where a uniform random error was added to the p_j values (Eq. (5)). As seen in Fig. 8b, the added noise essentially masked out distinguishing knowledge about the lowest $p_{j\ est}$ values, so that the hypervolume estimates stayed much larger than zero for even the lowest-risk estimates. Potentially, these errors could be reduced by truncation of the distributions (Levy, 1992) or via bootstrapping (Davidson and Duclos, 2006).

4.2. Potential use for the assessments based on model ensemble predictions

The hypervolume approach addresses a common problem of ensemble model predictions. When a distribution of estimates is generated by models with qualitatively distinct properties, simply averaging these estimates is inappropriate (Demeritt et al., 2007; Makridakis and Winkler, 1983). A good example of this situation is the assessment of impacts of a changing climate, where a set of future projections is generated with different families of General Circulation Models (GCMs). Currently, the Intergovernmental Panel on Climate Change (IPCC, 2014) reports projections for about a dozen future scenarios based on different GCMs and greenhouse gas emissions scenarios (IPCC, 2010a). Much research is being done on estimating future environmental risks under these various scenarios (Oppenheimer et al., 2014), but the main findings are often presented only in terms of selected scenarios (IPCC, 2010b).

A number of multi-model ensemble methods have been proposed to summarize findings across climate change scenarios

(Araújo and New, 2006). Such methods have shortcomings that have made them subject to criticism (see Collins, 2007; Tebaldi and Knutti, 2007). Our HV approach can be used to prioritize risk from model ensemble forecasts by estimating the HV measures based on the entire set of scenarios comprising the ensemble. Because the prioritization is done via pairwise FSD tests, there is no need to define the expected mean values over the ensemble set, especially since the FSD calculations integrate all variation between the scenarios in the set. This will be an area of our future work.

5. Conclusions

The proposed hypervolume approach addresses the difficult problem of prioritizing uncertain environmental and ecological risks in a geographical space (or "risk mapping", see Venette et al., 2010). Overall, the methodology offers a strategy for dealing with the typical problem of combining uncertain assessments of pest invasion risk into a one-dimensional risk estimate and generating risk priorities based on imprecise data. Because the uncertainty is incorporated directly into the risk measure via pairwise stochastic dominance tests, the approach helps address the preference of many decision-makers for a single risk-priority metric that they can use to allocate response measures. The HV metric is a continuous measure and thus can be used to compare assessments made with different datasets and assumptions.

Appendix A. Supplementary data

Supplementary data related to this article can be found at http://dx.doi.org/10.1016/j.jenvman.2017.02.021.

References

Apostolakis, G.E., 2004. How useful is quantitative risk assessment? Risk Anal. 24 (3), 515–520.

Araújo, M.B., New, M., 2006. Ensemble forecasting of species distributions. Trends Ecol. Evol. 22 (1), 42–47.

Aukema, J.E., Leung, B., Kovacs, K., Chives, C., Britton, K.O., Englin, J., Frankel, S.J., Haight, R.G., Holmes, T.P., Liebhold, A.M., McCullough, D.G., Von Holle, B., 2011. Economic impacts of non-native forest insects in the continental United States. PLoS One 6 (9), e24587.

Aven, T., 2010. On the need for restricting the probabilistic analysis in risk assessments to variability. Risk Anal. 30 (3), 354–360.

Aven, T., Zio, E., 2014. Foundational issues in risk assessment and risk management. Risk Anal. 34 (7), 1164–1172.

Back, T., Fogel, D., Michalewicz, Z. (Eds.), 1997. Handbook of Evolutionary Computation. Institute of Physics Publishing and Oxford University Press.

Beume, N., Naujoks, B., Emmerich, T., 2007. SMS-EMOA: multiobjective selection based on dominated hypervolume. Eur. J. Oper. Res. 181, 1653–1669.

Bradstreet, L., While, L., Barone, L., 2008. A fast incremental hypervolume algorithm. IEEE Trans. Evol. Comput. 12 (6), 714–723.

Bradstreet, L., While, L., Barone, L., 2010. A fast many-objective hypervolume algorithm using iterated incremental calculations. In: 2010 IEEE Congress on Evolutionary Computation, CEC, July 2010. IEEE Press, pp. 179–186.

Bringmann, K., Friedrich, T., 2010. An efficient algorithm for computing hypervolume contributions. Evol. Comput. 18, 383–402.

Brockhoff, D., Friedrich, T., Neumann, F., 2008. Analyzing hypervolume indicator based algorithms. In: Rudolph, G., Jansen, Th., Lucas, S.M., Poloni, C., Beume, N. (Eds.), Parallel Problem Solving from Nature X, LNCS 5199. Springer-Verlag Berlin, Heidelberg, pp. 651–660.

Brugnach, M., Tagg, A., Keil, F., de Lange, W.J., 2007. Uncertainty matters: computer models at the science-policy interface. Water Resour. Manag. 21 (7), 1075–1090.

Buck, J.H., Marshall, J.M., 2008. Hitchhiking as a secondary dispersal pathway for adult emerald ash borer, *Agrilus planipennis*. Gt. Lakes. Entomol. 41 (1–2), 197–198.

Canadian Food Inspection Agency (CFIA), 2013. Asian Long-horned Beetle Eradicated from Canada - News Release. Available from: http://www.inspection.gc.ca/about-the-cfia/newsroom/news-releases/2013-04-05/eng/1365168144940/1365168154936.

Canadian Food Inspection Agency (CFIA), 2014. *Anoplophora Glabripennis* (Motschulsky) - Asian Longhorned Beetle - Fact Sheet. Available from: http://www.inspection.gc.ca/plants/plant-pests-invasive-species/insects/asian-longhorned-beetle/fact-sheet/eng/1447168284946/1447168408039.

Canessa, S., Ewen, J.G., McCarthy, M.A., Walshe, T.V., 2016. Stochastic dominance to account for uncertainty and risk in conservation decisions. Conserv. Lett. 9 (4), 260–266.

Carrasco, L.R., Baker, R., MacLeod, A., Knight, J.D., Mumford, J.D., 2010. Optimal and robust control of invasive alien species spreading in homogeneous landscapes. J. R. Soc. Interface 7, 529–540.

Carter, M.E., Smith, M.T., Turgeon, J.J., Harrison, R.G., 2009. Analysis of genetic diversity in an invasive population of Asian longhorned beetles in Ontario, Canada. Can. Entomol. 141, 582–594.

Cheung, K.K.W., 2001. A review of ensemble forecasting techniques with a focus on tropical cyclone forecasting. Meteorol. Appl. 8, 315–332.

Cohen, S., Guibas, L., 1997. The Earth Mover's Distance: Lower Bounds and Invariance under Translation. Technical Report STAN-CS-TR-97-1597. Stanford University, Computer Science Department. Available from: http://i.stanford.edu/pub/cstr/reports/cs/tr/97/1597/CS-TR-97-1597.pdf.

Collins, M., 2007. Ensembles and probabilities: a new era in the prediction of climate change. Philos. Trans. R. Soc. A 365, 1957–1970.

Cook, G., Downing, M., 2013. Traffic Pattern Project Report: Methodology for Interpolating Traffic Count Data to a Road Network. USDA Animal Plant Health Inspection Service, Plant Protection and Quarantine, Centre for Plant Health Science and Technology, Fort Collins, CO.

Davidson, R., Duclos, J.-Y., 2006. Testing for Restricted Stochastic Dominance. CIRPEE Working Paper 06–09. Available from: http://papers.ssrn.com/sol3/papers.cfm?abstract_id=894282.

De Giorgi, E., 2002. Reward-risk Portfolio Selection and Stochastic Dominance. Working paper. Available from: https://ideas.repec.org/p/zur/iewwpx/121.html.

Deb, K., Mohan, M., Mishra, S., 2005. Evaluating the ε-domination based multi-objective evolutionary algorithm for a quick computation of Pareto-optimal solutions. Evol. Comput. 13 (4), 501–525.

Demeritt, D., Cloke, H., Pappenberger, F., Thielen, J., Bartholomes, J., Ramos, M., 2007. Ensemble predictions and perceptions of risks, uncertainty, and errors in flood forecasting. Environ. Hazards 7 (2), 115–127.

Elton, E.J., Gruber, M.J., 1995. Modern Portfolio Theory and Investment Analysis, fifth ed. Wiley, New York, NY.

Emmerich, M., Beume, N., Naujoks, B., 2005. An EMO algorithm using the hypervolume measure as selection criterion. In: Coello, C.A., Hernandez Aguirre, A., Zitzler, E. (Eds.), Evolutionary Multi-criterion Optimization. Third International Conference, EMO, 2005, Guanajuato, Mexico. Springer Lecture Notes in Computer Science, vol. 3410, pp. 62–76.

Environmental Systems Research Institute (ESRI), 2014. Street Map Premium for ArcGIS. Available from:http://www.esri.com/data/streetmap.

EPPO (European and Mediterranean Plant Protection Organization), 2008. EPPO Reporting Service, No. 5. Available at: http://archives.eppo.org/EPPOReporting/2008/Rse-0805.pdf.

Faccoli, M., Favaro, R., 2016. Host preference and host colonization of the Asian long-horned beetle *Anoplophora glabripennis* (Coleoptera Cerambycidae). In: Southern Europe. Bulletin of Entomological Research. http://dx.doi.org/10.1017/S0007485315001157.

Favaro, R., Wichmann, L., Ravn, H.P., Faccoli, M., 2015. Spatial spread and infestation risk assessment in the Asian longhorned beetle, *Anoplophora glabripennis*. Entomol. Exp. Appl. 155 (2), 95–101.

Fishburn, P.C., Vickson, R.C., 1978. Theoretical foundations of stochastic dominance. In: Whitemore, G.A., Findlay, M.C. (Eds.), Stochastic Dominance. An Approach to Decision-making under Risk. Lexington Books, D.C. Heath and Co, Lexington, MA, pp. 39–144.

Fleischer, M., 2003. The measure of Pareto optima. Applications to multi-objective metaheuristics. In: Fonseca, C.M., Fleming, P.J., Zitzler, E., Deb, K., Thiele, L. (Eds.), Evolutionary Multi-criterion Optimization. Second International Conference, EMO 2003, Faro, Portugal, vol. 2632. Springer. Lecture Notes in Computer Science, pp. 519–533.

Fonseca, C.M., Paquete, L., Lopez-Ibanez, M., 2006. An improved dimension-sweep algorithm for the hypervolume indicator. In: 2006 IEEE Congress on Evolutionary Computation (CEC), July 2006, Vancouver, BC, Canada. IEEE Press, pp. 3973–3979.

Gerber, H.U., Pafumi, G., 1998. Utility functions: from risk theory to finance. North Am. Actuar. J. 2, 74–100.

Goerlandt, F., Montewka, J., Kuzmin, V., Kujala, P., 2015. A risk-informed ship collision alert system: framework and application. Saf. Sci. 77, 182–204.

Goldberg, D.E., 1989. Genetic Algorithms in Search, Optimization, and Machine Learning. Addison-Wesley Publ. Co, Reading, MA.

Haack, R.A., Cavey, J.F., Hoebeke, E.R., Law, K., 1996. *Anoplophora glabripennis*: a new tree-infesting exotic cerambycid invades New York. Newsl. Mich. Entomol. Soc. 41 (2–3), 1–3.

Haack, R.A., Law, K.R., Mastro, V.C., Ossenbruggen, H.S., Raimo, B.J., 1997. New York's battle with the Asian longhorned beetle. J. For. 95, 11–15.

Hester, S.M., Brooks, S., Cacho, O.J., Panetta, F.D., 2010. Applying a simulation model to the management of an infestation of Miconia calvescens in the wet tropics of Australia. Weed Res. 50, 269–279.

Haack, R.A., Heerard, F., Sun, J., Turgeon, J.J., 2010. Managing invasive populations of Asian longhorned beetle and citrus longhorned beetle: a worldwide perspective. Annu. Rev. Entomol. 55, 521–546.

Hopkin, A., de Groot, P., Turgeon, J.J., 2004. Alien forest insects: what's bugging us in Ontario? Emerald ash borer and Asian longhorned beetle. For. Health Biodivers. News 8 (5), 1–2.

Hu, J., Angeli, S., Schuetz, S., Luo, Y., Hajek, A.E., 2009. Ecology and management of exotic and endemic Asian longhorned beetle *Anoplophora glabripennis*. Agric. For. Entomol. 11, 359–375.

Huband, S., Hingston, P., White, L., Barone, L., 2003. An evolution strategy with probabilistic mutation for multi-objective optimisation. In: Congress on Evolutionary Computation (CEC 2003), vol. 3. IEEE Press, Canberra, Australia, pp. 2284–2291.

Intergovernmental Panel on Climate Change (IPCC), 2010a. IPCC Cross-working Group Meeting on Consistent Treatment of Uncertainties. Guidance Note for Lead Authors of the IPCC Fifth Assessment Report on Consistent Treatment of Uncertainties. Jasper Ridge, CA, USA, 6–7 July 2010. Core Writing Team: Mastrandrea, M.D., Field, C.B., Stocker, T.F., Edenhofer, O., Ebi, K.L., Frame, D.J., Held, H., Kriegler, E., Mach, K.J., Matschoss, P.R., Plattner, G.-K., Yohe, G.W., Zwiers, F.W.J. Available from: https://www.ipcc.ch/pdf/supporting-material/uncertainty-guidance-note.pdf.

Intergovernmental Panel on Climate Change (IPCC), 2010b. In: Stocker, T., Dahe, Q., Plattner, G.-K., Tignor, M., Midgley, P. (Eds.), IPCC Expert Meeting on Assessing and Combining Multi Model Climate Projections National Center for Atmospheric Research. Boulder, Colorado, USA, 25–27 January 2010. IPCC Working Group I Technical Support Unit, University of Bern, Bern, Switzerland. Available from: https://www.ipcc.ch/pdf/supporting-material/expert-meeting-assessing-multi-model-projections-2010-01.pdf.

Intergovernmental Panel on Climate Change (IPCC), 2014. In: Pachauri, R.K., Meyer, L.A. (Eds.), Climate Change 2014: Synthesis Report. Contribution of Working Groups I, II and III to the Fifth Assessment Report of the Intergovernmental Panel on Climate Change. IPCC, Geneva, Switzerland.

Jorion, P., 1997. Value at Risk: the New Benchmark for Controlling Derivatives Risk. Irwing Publ., Chicago, IL.

Kaplan, S., Garrick, B.J., 1981. On the quantitative definition of risk. Risk Anal. 1, 11–27.

Keisler, J.M., Linkov, I., 2010. Managing a portfolio of risks. In: Cochran, J.J. (Ed.), Wiley Encyclopedia of Operations Research and Management Science. John Wiley & Sons (e-book), pp. 1–24.

Knowles, J., Corne, D., 2002. On metrics for comparing non-dominated sets. In: Congress on Evolutionary Computation (CEC 2002). NJ. IEEE Press, Piscataway, pp. 711–716.

Knowles, J., Corne, D., Fleischer, M., 2006. Bounded archiving using the Lebesgue measure. In: Congress on Evolutionary Computation (CEC) 2003. IEEE Press, Canberra, Australia, pp. 2490–2497.

Koch, F.H., Yemshanov, D., McKenney, D.W., Smith, W.D., 2009. Evaluating critical uncertainty thresholds in a spatial model of forest pest invasion risk. Risk Anal. 29 (9), 1227–1241.

Kuiper, N.H., 1962. Tests concerning random points on a circle. Proc. Koninklijke Nederl. Akademie van Wetenschappen, Ser. A 63, 38–47.

Laumanns, M., Zitzler, E., Thiele, L., 2000. A unified model for multi-objective evolutionary algorithms with elitism. In: 2000 Congress on Evolutionary Computation, July 2000, vol. 1. IEEE Service Center, Piscataway, NJ, pp. 46–53.

Levy, H., 1992. Stochastic dominance and expected utility: survey and analysis. Manag. Sci. 38 (4), 555–593.

Levy, H., 1998. Stochastic Dominance: Investment Decision Making under Uncertainty. Kluwer Academic Publishers, Boston, MA.

Lingafelter, S.W., Hoebeke, E.R., 2002. Revision of Anoplophora (Coleoptera: Cerambycidae). Entomological Society of Washington.

Linkov, I., Satterstrom, F.K., Kiker, G., Seager, T.P., Bridges, T., Gardner, K.H., Rogers, S.H., Belluck, D.A., Meyer, A., 2006. Multicriteria decision analysis: a comprehensive decision approach for management of contaminated sediments. Risk Anal. 26, 61–78.

Makridakis, S., Winkler, R.L., 1983. Averages of forecasts: some empirical results. Manag. Sci. 29, 987–996.

Markowitz, H., 1952. Portfolio selection. J. Finance 7, 77–91.

Maspero, M., Jucker, C., Colombo, M., 2007. First record of *Anoplophora glabripennis* (Motschulsky) (Coleoptera: Cerambycidae, Lamiinae, Lamiini) in Italy. Boll. Zool. Agrar. Bachic. 39, 161–164.

Melbourne, B.A., Hastings, A., 2009. Highly variable spread rates in replicated biological invasions: fundamental limits to predictability. Science 325 (5947), 1536–1539.

Meng, P.S., Hoover, K., Keena, M.A., 2015. Asian longhorned beetle (Coleoptera: Cerambycidae), an introduced pest of maple and other hardwood trees in North America and Europe. J. Integr. Pest Manag. 6, 4. http://dx.doi.org/10.1093/jipm/pmv003.

Meyerson, L.A., Reaser, J.K., 2003. Bioinvasions, bioterrorism, and biosecurity. Front. Ecol. Environ. 1 (3), 307–314.

Nehme, M.E., Trotter, R.T., Keena, M.E., McFarland, C., Coop, J., Hull-Sanders, H.M., Meng, P., De Moraes, D.M., Mescher, M.C., Hoover, K., 2014. Development and evaluation of a trapping system for *Anoplophora glabripennis* (Coleoptera: Cerambycidae) in the United States. Environ. Entomol. 43, 1034–1044.

Nowak, D.J., Pasek, J.E., Sequeira, R.A., Crane, D.E., Mastro, V.C., 2001. Potential effect of *Anoplophora glabripennis* (Coleoptera: Cerambycidae) on urban trees in the United States. J. Econ. Entomol. 94, 116–122.

Oppenheimer, M., Campos, M., Warren, R., Birkmann, J., Luber, G., O'Neill, B., Takahashi, K., 2014. Emergent risks and key vulnerabilities. In: Field, C.B., Barros, V.R., Dokken, D.J., Mach, K.J., Mastrandrea, M.D., Bilir, T.E., Chatterjee, M., Ebi, K.L., Estrada, Y.O., Genova, R.C., Girma, B., Kissel, E.S., Levy, A.N., MacCracken, S., Mastrandrea, P.R., White, L.L. (Eds.), Climate Change 2014: Impacts, adaptation, and Vulnerability. Part A: Global and Sectoral aspects. Contribution of Working Group II to the Fifth Assessment Report of the Intergovernmental Panel on Climate Change. Cambridge University Press, Cambridge, United Kingdom and New York, NY, USA, pp. 1039–1099. Available from: https://ipcc-wg2.gov/AR5/images/uploads/WGIIAR5-Chap19_FINAL.pdf.

Pareto, V., 1971. Manual of Political Economy. Augustus M. Kelley, New York. Translated from 1927 French edition by Ann S. Schwier.

Paté-Cornell, M.E., 1996. Uncertainties in risk analysis: six levels of treatment. Reliab. Eng. Syst. Saf. 54, 95–111.

Peacock, J., 1983. Two-dimensional goodness-of-fit testing in astronomy. Mon. Not. R. Astronomical Soc. 202, 615–627.

Peterson, A.T., Scachetti-Pereira, R., 2004. Potential geographic distribution of *Anoplophora glabripennis* (Coleoptera: Cerambycidae) in North America. Am. Midl. Nat. 151 (1), 170–178.

Poland, T.M., Haack, R.A., Petrice, T.R., 1998. Chicago Joins New York in battle with the Asian longhorned beetle. Newsl. Mich. Entomol. Soc. 43 (4), 15–17.

Rubner, Y., Tomasi, C., Guibas, L.J., 2000. The earth mover's distance as a metric for image retrieval. Int. J. Comput. Vis. 40 (2), 99–121.

Salo, A., Keisler, J., Morton, A., 2011. An invitation to portfolio decision analysis. In: Salo, A., Keisler, J., Morton, A. (Eds.), Portfolio Decision Analysis: Improved Methods for Resource Allocation. Springer Science, New York, NY, pp. 3–27.

Schneider, S.H., Semenov, S., Patwardhan, A., Burton, I., Magadza, C.H.D., Oppenheimer, M., Pittock, A.B., Rahman, A., Smith, J.B., Suarez, A., Yamin, F., 2007. Assessing key vulnerabilities and the risk from climate change. Climate Change 2007: Impacts, Adaptation and Vulnerability. In: Parry, M.L., Canziani, O.F., Palutikof, J.P., van der Linden, P.J., Hanson, C.E. (Eds.), Contribution of Working Group II to the Fourth Assessment Report of the Intergovernmental Panel on Climate Change. Cambridge University Press, Cambridge, UK, pp. 779–810.

Shatz, A.J., Rogan, J., Sangermano, F., Ogneva-Himmelberger, Y., Chen, H., 2013. Characterizing the potential distribution of the invasive Asian longhorned beetle (*Anoplophora glabripennis*) in Worcester County, Massachusetts. Appl. Geogr. 45, 259–268.

Sims, C., Finnof, D., 2013. When is a "wait and see" approach to invasive species justified? Resour. Energy Econ. 35, 235–255.

Smirnov, N., 1948. Table for estimating the goodness of fit of empirical distributions. Ann. Math. Stat. 19, 279–281.

Smith, K., 2013. Environmental Hazards: Assessing Risk and Reducing Disaster, sixth ed. Routledge, New York NY.

Smith, M.T., Bancroft, J., Li, G.H., Gao, R.T., Teale, S., 2001. Dispersal of *Anoplophora glabripennis* (Cerambycidae). Environ. Entomol. 30 (6), 1036–1040.

Smith, M.T., Tobin, P., Bancroft, J.S., Li, G.H., Gao, R.T., 2004. Dispersal and spatiotemporal dynamics of Asian longhorned beetle (Coleoptera: Cerambycidae) in China. Environ. Entomol. 33, 435–442.

Smith, M.T., Wu, J.Q., 2008. Asian longhorned beetle: renewed threat to northeastern USA and implications worldwide. Int. Pest Control 50, 311–316.

Standing Advisory Committee for Trunk Road Assessment (SACTRA), 1999. Transport and the Economy: Full Report (SACTRA). Available from: http://webarchive.nationalarchives.gov.uk/20050301192906/http:/dft.gov.uk/stellent/groups/dft_econappr/documents/pdf/dft_econappr_pdf_022512.pdf.

Straw, N., Fielding, N., Tilbur, C., Williams, D., Inward, D., 2015. Host plant selection and resource utilisation by Asian longhorned beetle *Anoplophora glabripennis* (Coleoptera: Cerambycidae) in southern England. Forestry 88, 84–95.

Straw, N.A., Fielding, N.J., Tilbury, C., Williams, D.T., Cull, T., 2016. History and development of an isolated outbreak of Asian longhorn beetle *Anoplophora glabripennis* (Coleoptera: Cerambycidae) in southern England. Agric. For. Entomol. http://dx.doi.org/10.1111/afe.12160.

Tebaldi, C., Knutti, R., 2007. The use of the multi-model ensemble in probabilistic climate projections. Philos. Trans. R. Soc. A 365, 2053–2075.

Tetrad Inc, 2014. TrafficMetrix Canada. Official website: http://www.tetrad.com/maps_and_data/canada/traffic/.

Trotter III, E.T., Hull-Sanders, H.M., 2015. Quantifying dispersal of the Asian longhorned beetle (*Anoplophora glabripennis*, Coleoptera) with incomplete data and behavioral knowledge. Biol. Invasions. http://dx.doi.org/10.1007/s10530-015-0961-9.

Turgeon, J.J., Ric, J., de Groot, P., Gasman, B., Orr, M., Doyle, J., Smith, M.T., Dumouchel, L., Scarr, T., 2007. Détection des signes et symptômes d'attaque par le longicorne étoilé: Guide de formation. Gouvernement du Canada, Sault Ste. Marie, ON, Canada. Available from: http://cfs.nrcan.gc.ca/pubwarehouse/pdfs/26861.pdf.

Turgeon, J.J., Pedlar, J., de Groot, P., Smith, M.T., Jones, C., Orr, M., Gasman, B., 2010. Density and location of simulated signs of injury affect efficacy of ground surveys for Asian longhorned beetle. Can. Entomol. 142, 80–96.

Turgeon, J.J., Orr, M., Grant, C., Wu, Y., Gasman, B., 2015. Decade-old satellite infestation of *Anoplophora glabripennis* Motschulsky (Coleoptera: Cerambycidae) found in Ontario, Canada outside regulated area of founder population. Coleopt. Bull. 69, 674–678.

USDA Animal Plant Health Inspection Service (APHIS), 2005. Asian Longhorned Beetle (Anoplophora Glabripennis) Fact Sheet. United States Department of Agriculture, Animal Plant Health Inspection Service, January 2005. Available from: http://www.aphis.usda.gov/lpa/pubs/fsheet_faq_notice/fs_phalb.pdf.

USDA Animal Plant Health Inspection Service (APHIS), 2013. Asian Longhorned Beetle Cooperative Eradication Program in Clermont County, Ohio. 2013. Available from: http://www.aphis.usda.gov/plant_health/ea/downloads/2013/OHClermontCountyRevised_EA_May_final.pdf.

van der Gaag, D.J., Loomans, J.M., 2014. Host plants of *Anoplophora glabripennis*, a review. Eur. Mediterr. Plant Prot. Organ. Bull. 44, 518–528.

Venette, R.C., Kriticos, D.J., Magarey, R., Koch, F., Baker, R.H.A., Worner, S., Gómez, N.N., McKenney, D., Dobesberger, E.J., Yemshanov, D., De Barro, P.,

Hutchison, W.D., Fowler, G., Kalaris, T., Pedlar, J., 2010. Pest risk maps for invasive alien species: a roadmap for improvement. BioScience 60, 349–362.
Walker, W.E., Harremoës, P., Rotmans, J., van der Sluijs, J.P., van Asselt, M.B.A., Janssen, P., Krayer von Krauss, M.P., 2003. Defining uncertainty: a conceptual basis for uncertainty management in model-based decision support. Integr. Assess. 4 (1), 5–17.
Wang, B., Mastro, V.C., Gao, R.T., 2005. Host range of *Anoplophora glabripennis*: what we've learned from common-garden experiment data. In: Fosbroke, S.L.C., Gottschalk, K.W. (Eds.), 16th U.S. Department of Agriculture Interagency Research Forum on Gypsy Moth and Other Invasive Species. Newtown Square, PA, USDA Forest Service General Technical Report. NE-GTR-337, p. 89.
While, L., Bradstreet, L., Barone, L., Hingston, P., 2005. Heuristics for optimising the calculation of hypervolume for multi-objective optimisation problems. In: 2005 IEEE Congress on Evolutionary Computation (CEC 2005), vol. 3. IEEE, pp. 2225–2232.
While, L., Hingston, P., Barone, L., Huband, S., 2006. A faster algorithm for calculating hypervolume. IEEE Trans. Evol. Comput. 10 (1), 29–38.
White, D.D., Wutich, A.Y., Larson, K.L., Lant, T., 2015. Water management decision makers' evaluations of uncertainty in a decision support system: the case of WaterSim in the Decision Theater. J. Environ. Plan. Manag. 58 (4), 616–630.
Williams, D.W., Lee, H.-P., Kim, I.-K., 2004. Distribution and abundance of *Anoplophora glabripennis* (Coleoptera: Cerambycidae) in natural Acer stands in South Korea. Environ. Entomol. 33, 540–545.
Wu, J., Azarm, S., 2001. Metrics for quality assessment of a multiobjective design optimization solution set. Transactions of the ASME. J. Mech. Des. 123, 18–25.
Yemshanov, D., Koch, F.H., McKenney, D.W., Downing, M.C., Sapio, F., 2009. Mapping invasive species risks with stochastic models: a cross-border United States-Canada application for *Sirex noctilio* Fabricius. Risk Anal. 29, 868–884.
Yemshanov, D., Koch, F.H., Lyons, B., Ducey, M., Koehler, K., 2012. A dominance-based approach to map risks of ecological invasions in the presence of severe uncertainty. Divers. Distrib. 18, 33–46.
Yemshanov, D., Koch, F.H., Ben-Haim, Y., Downing, M., Sapio, F., 2013. A new multi-criteria risk mapping approach based on a multi-attribute frontier concept. Risk Anal. 33, 1694–1709.
Yemshanov, D., Koch, F.H., Ducey, M., 2015. Making invasion models useful for decision makers: incorporating uncertainty, knowledge gaps, and decision-making preferences. In: Venette, R.C. (Ed.), Pest Risk Modelling and Mapping for Invasive Alien Species. CABI, Oxfordshire, UK, pp. 206–222.
Zhou, Q., Lambert, J.H., Karvetski, C.W., Keisler, J.M., Linkov, I., 2012. Flood protection diversification to reduce probabilities of extreme losses. Risk Anal. 32, 1873–1887.
Zitzler, E., 2001. Hypervolume Metric Calculation. Available from: ftp://ftp.tik.ee.ethz.ch/pub/people/zitzler/hypervol.c.
Zitzler, E., Thiele, L., 1998. Multiobjective optimization using evolutionary algorithms - a comparative case study. In: Conference on Parallel Problem Solving from Nature (PPSN V), Amsterdam, pp. 292–301.
Zitzler, E., Thiele, L., 1999. Multiobjective evolutionary algorithms: a comparative case study and the strength Pareto approach. IEEE Trans. Evol. Comput. 3 (4), 257–271.
Zitzler, E., Thiele, L., Laumanns, M., Fonseca, C.M., da Fonseca, V.G., 2003. Performance assessment of multiobjective optimizers: an analysis and review. IEEE Trans. Evol. Comput. 7 (2), 117–132.